Electronic Supplementary Material (ESI) for Materials Horizons.

Liquid layer generator for excellent icephobicity at extremely low temperature

Feng Wang[a], Senbo Xiao[a], Yizhi Zhuo[a], Wenwu Ding[b], Jianying He[a,*], Zhiliang Zhang[a,*]

a. NTNU Nanomechanical Lab, Department of Structural Engineering, Norwegian University of Science and Technology (NTNU), Trondheim 7491, Norway.

b. Department of Energy and Process Engineering, Norwegian University of Science and Technology (NTNU), Trondheim 7491, Norway.

*E-mail: jianying.he@ntnu.no, zhiliang.zhang@ntnu.no

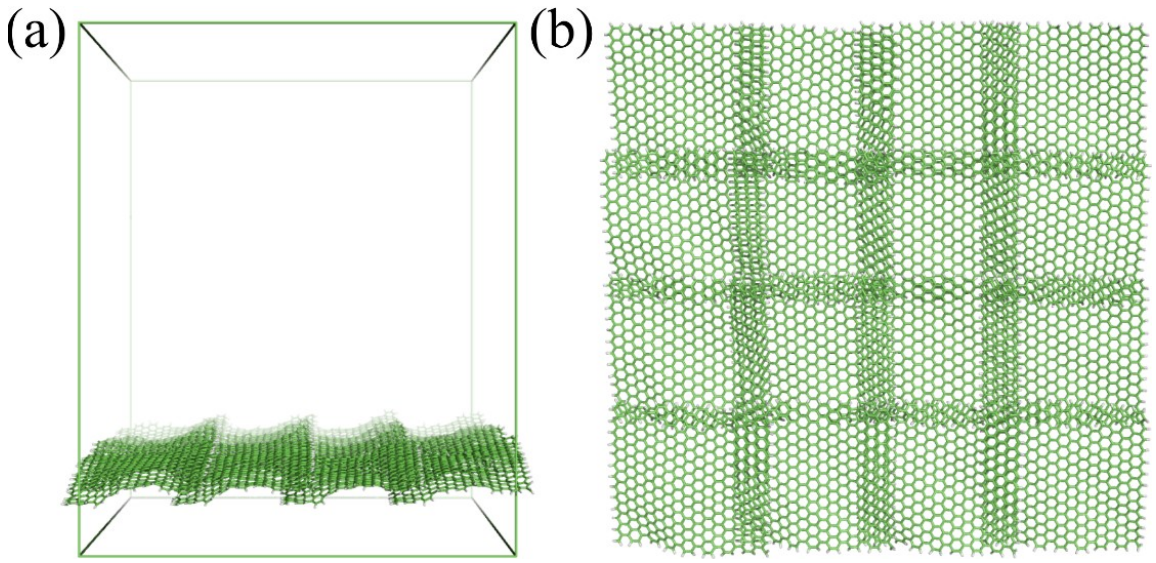

Supplementary Figure S1 | Side (a) and top (b) views of the carbon-based substrate consisting of graphene platelets. The graphene platelets had a uniform size of 2.3 nm × 2.3 nm, and were periodically fixed at equilibrium positions with an overlapping margin of 0.6 nm.

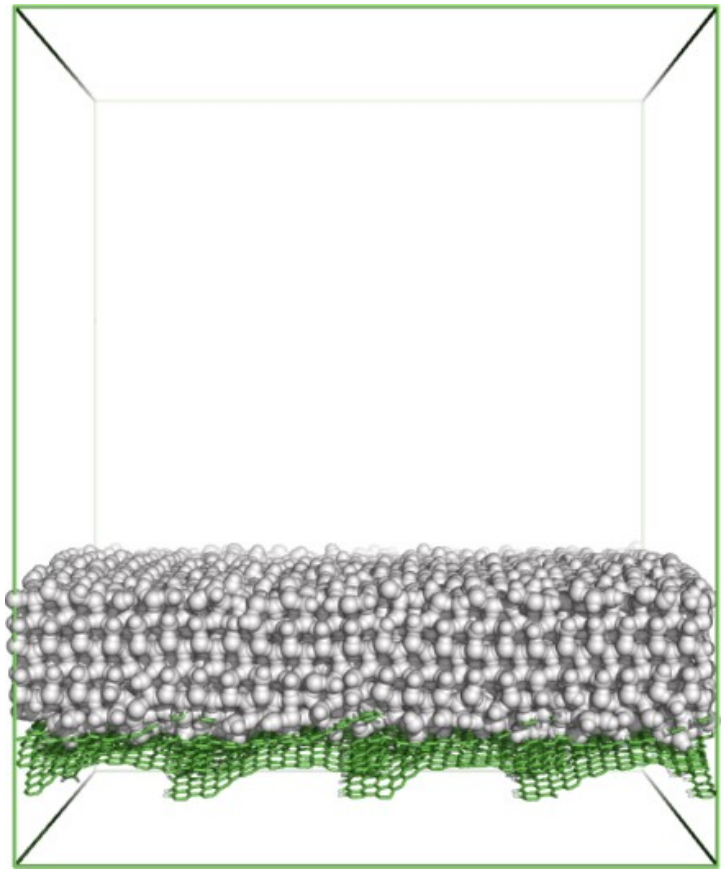

Supplementary Figure S2 | Simulation system of ice directly contacts with substrate without any interfacial lubricating layer.

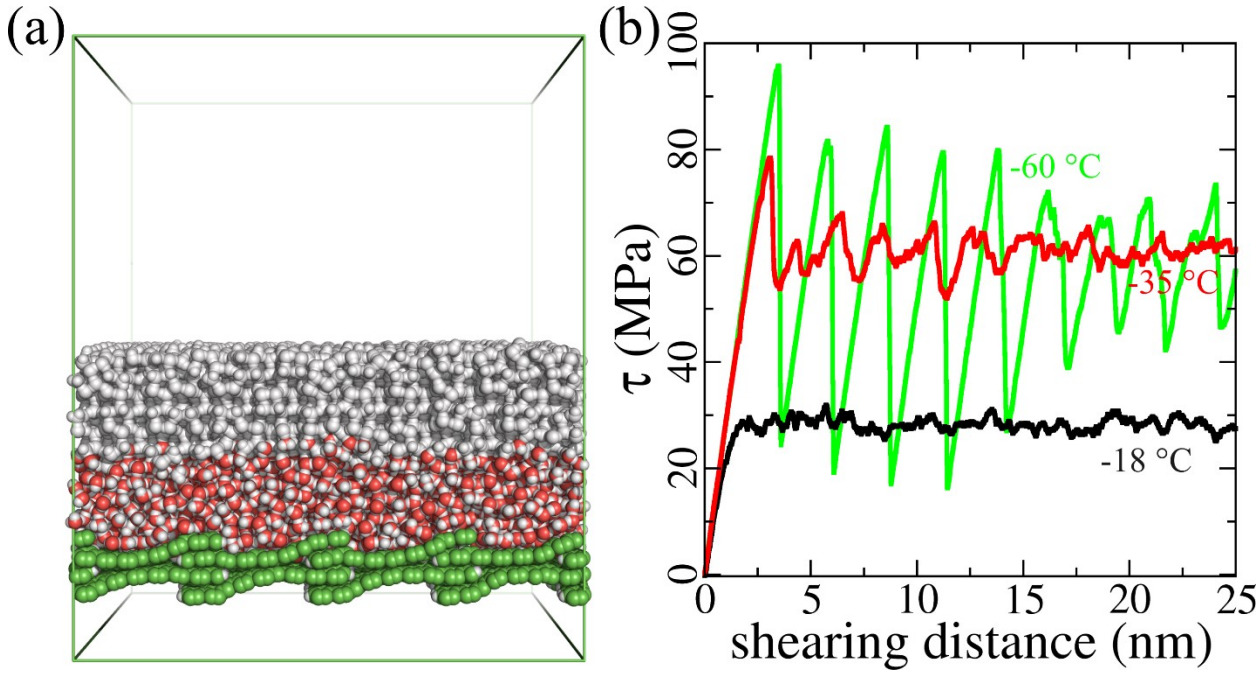

Supplementary Figure S3 | Lubricating effect of an interfacial water layer of 2 nm at varied temperature. (a) The all-atom simulation system. **(b)** Shearing stress, τ, profiles of ice at temperature of -18˚C, -35˚C and -60˚C, showing an increase pattern of average τ and losing of lubricating effect with decrease of temperature.

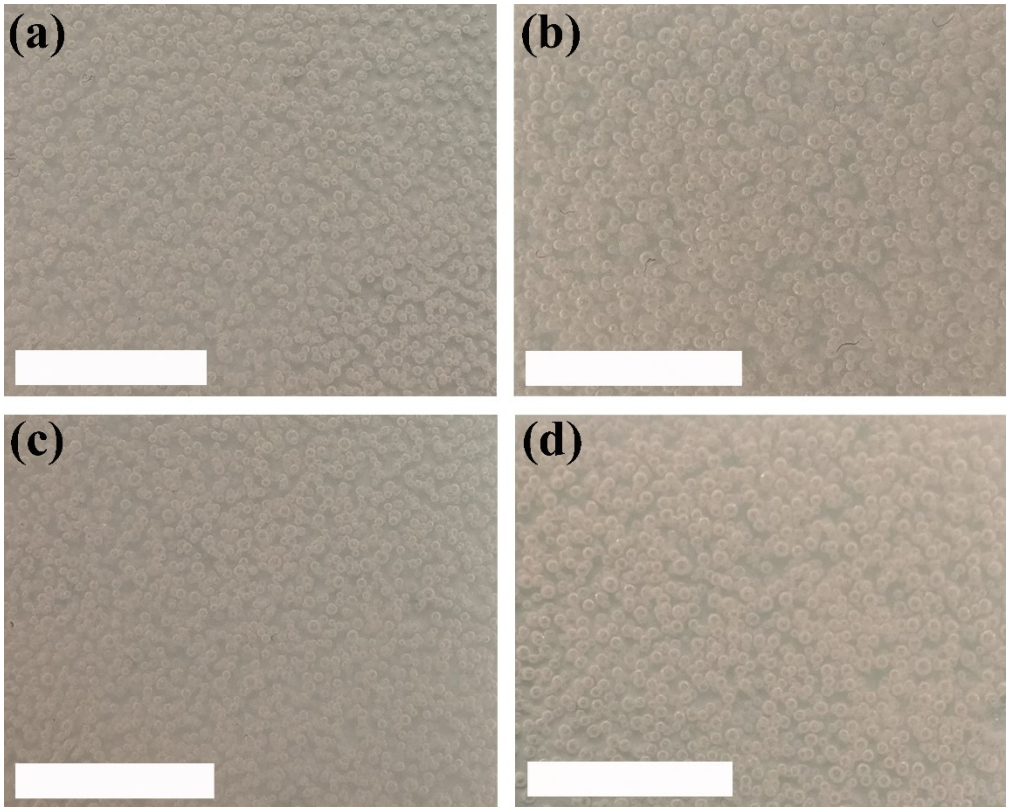

Supplementary Figure S4 | Optical images showing ethanol droplets in the LLG 1. (a) ~ (d) The samples with ethanol volume content of 10%, 20%, 30% and 40%, respectively. The droplets size shows a trend of increase with increasing ethanol content. The scale bar is 1mm in all images.

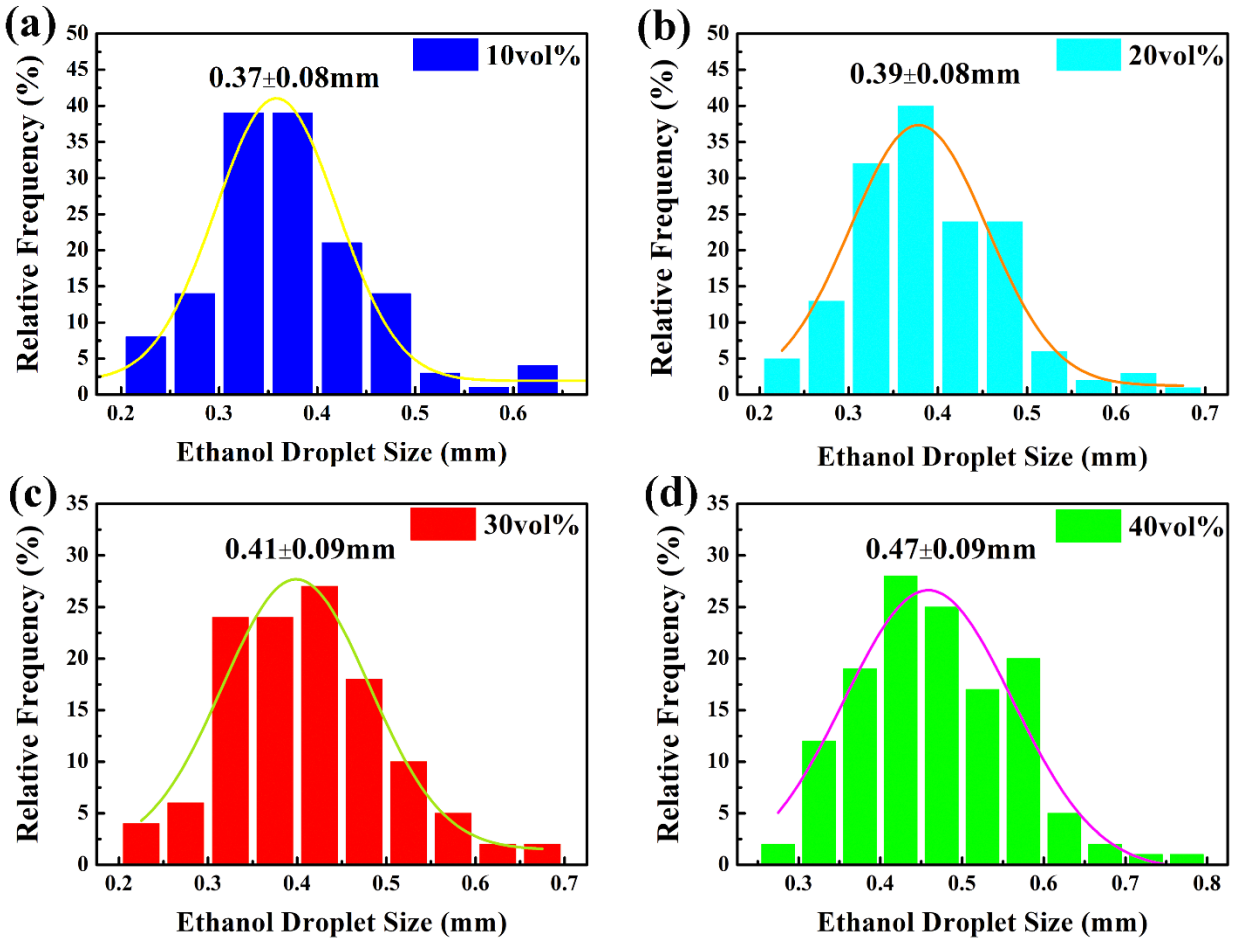

Supplementary Figure S5 | Size distribution of ethanol droplets in the LLG 1. The distribution was close to unimodal Gaussian distribution in all samples. With increasing ethanol content in the polymer, the droplet size increased.

The ice adhesion strength on the ethanol-exhausted sample was higher than that on the pure silicon rubber, which can be explained by the classic ice adhesion theory[1, 2]

$$\tau = \sqrt{\frac{EG}{\pi a \Lambda}} \qquad (1)$$

where E is Young's modulus of the substrate, G is the surface energy, a is the crack length, and Λ is a non-dimensional constant determined by the geometric configuration of the interface cracks. Pores were left in the substrates after the removal of ethanol droplets, which reduced Young's modulus and also acted as macro-crack initiators which could increase the crack length[3]. Both favored weakening ice adhesion strength. Yet importantly, in the curing process of LLG 1, the evaporation of ethanol droplets in the substrate introduced a significant increase in the surface roughness, as schematic shown in Fig. S6, which caused physical ice interlocking with the substrate. Obviously, interlocking outperformed the combining effect of lowering substrate apparent modulus and increased cracking initiators in the dry LLG 1[4]. Thus, the ethanol-exhausted samples shew higher ice adhesion strength.

However, the comparison among the ethanol-exhausted samples was more complex. With increasing ethanol content in LLG 1, obviously, the average pore size increase (Fig. S4 and Fig. S5). Firstly, the Young's modulus would decrease with increasing ethanol content consequently. Secondly, the macro-crack initiators effect was enhanced, which resulted in crack length improvement with increasing ethanol content. Both of them favored low ice adhesion strength along ethanol content[1], which counteract with the effect of increased surface roughness resulted from higher ethanol content (Fig. S6). Because it was hard to quantitatively determine and control which factors to be outperforming in the LLG samples with varied ethanol content, there is no clear trend observed in the ice adhesion results.

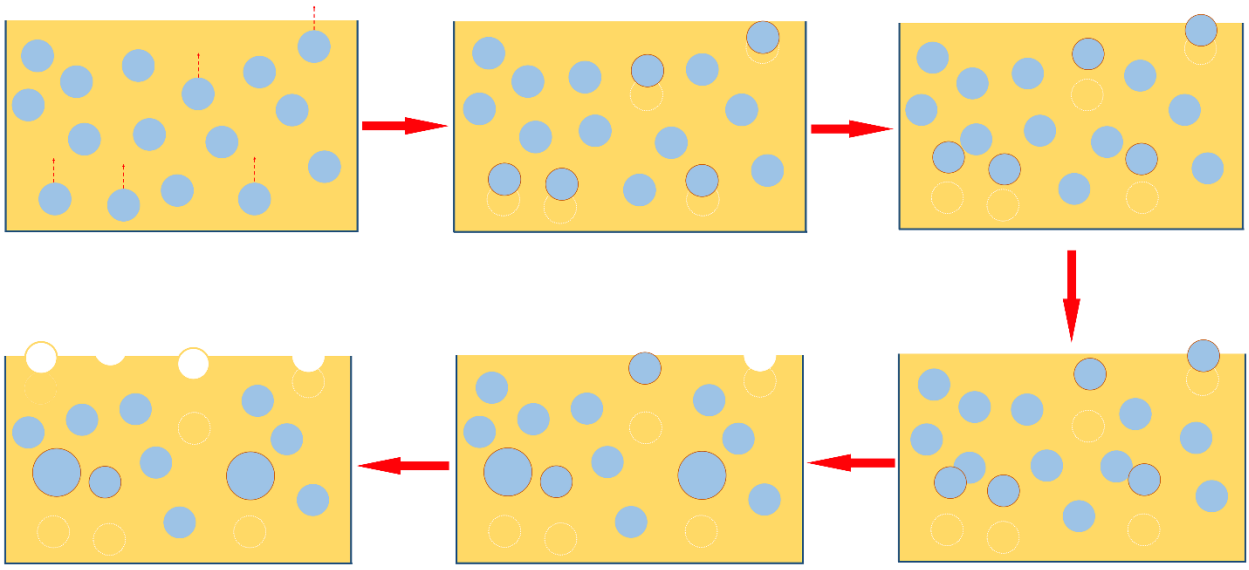

Supplementary Figure S6 | Schematic showing the formation process of the roughness on the LLG 1 surface. The ethanol droplets in the liquid polymer were initially in a metastable phase in the mixture. In the curing process, the ethanol droplets were able to coalesce with their neighbors and float to the surface, then released to the ambient. As the viscosity of the polymer increased with the on-going curing process, the remaining ethanol droplets on the surface created pores that contributed to the roughness of the surface. The surface roughness was proportional to the ethanol content.

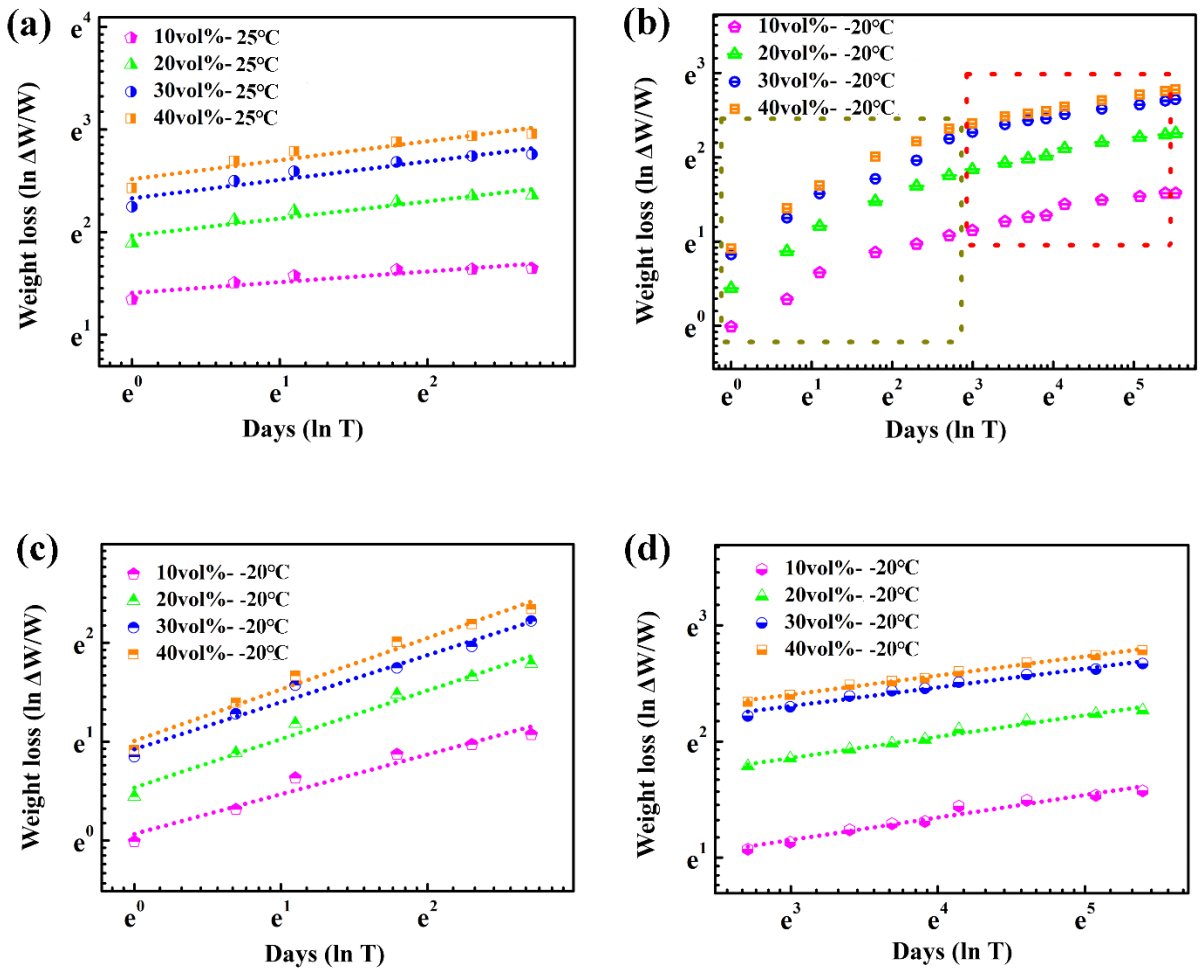

Supplementary Figure S7 | Weight loss of LLGs under different temperature. (a) Weight loss of LLGs at room temperature as a function of time. **(b)** Weight loss of LLGs at -20℃ as a function of time. **(c)** and **(d)** were the fitting curves of the points from left and right part of **(b).** The dot lines in all plots were the fitting curves.

The weight loss of the LLGs showed a linear relationship with time in the logarithm graphs. The relationship below was used to fit the weight loss data in the graphs:

$$\ln\frac{\Delta W}{W} = a + b\ln T \qquad (1)$$

where ΔW is the accumulated weight reduction of the LLGs, W is the initial weight of LLGs, and T ($T \geqslant 1$) is the holding time after fabrication. The constants a and b are determined by ethanol

content, temperature, pressure and other ambient factors. The values of *a* and *b* for different samples are given in Table 1.

There were two mechanisms causing the weight loss of LLGs, namely active secretion and passive diffusion. The ethanol molecules that were randomly trapped between the silicon rubber can be secreted by the polymer chains in a fast manner, while ethanol droplets sealed in the polymer body can only leak slowly by passive diffusion. As exemplified by data obtained under -20℃, two sets of constants *a* and *b* were needed for fitting the first and the second half of the data points (Fig. S7b). In the first stage of leaking, less than 15 days depicted by Fig. S7c, both active secretion and passive diffusion were functioning at the same time. Thus, higher ethanol leaking rates were detected, with higher value of b (samples 5 to 8 in Table 1). After 15 days and with the exhaustion of active secretion shown in Fig. S6d, the passive diffusion of ethanol dominated resulting in lower leaking rates (samples 9 to 12 in Table 1). The value of *b* among each series (1~4, 5~8, and 9~12) with different ethanol content was close, which meant similar leaking rate for silicon rubber with different ethanol content under the same temperature.

The constant *a* denotes the initial weight loss and correlates with the ethanol content in the LLG sample series (1~4, 5~8, and 9~12). The values of *a* were higher in Fig. S7a than Fig. S7c, which meant *a* was also proportional to the ambient temperature. It should be noted that the *a* in the Fig. S7c was not comparable with Fig. S7a and Fig. S7c for the different starting time.

By combining the final weight loss in Fig. S7a and the equation (1), we could calculate the lifespan of LLG 1 with various ethanol content. The experimental results in Fig. S7b at 250 day shew the weight of sample with 10vol% ethanol no more decrease, which agree well with the number in Table 2. Thus, we could reasonably believe the LLG 1 with 40vol% ethanol could continuously release ethanol for around 593 days.

It should be noted that the weight loss of ethanol in LLG 1 was not perfectly matched with the initial volume ration of the ethanol in the samples. The reason was that the weight was measured after silicon elastomer cured, not including the amount that had evaporated in the 3-hours long curing process of the LLG samples.

Table 1 | The number of a and b for different LLG 1 samples

Samples	Ethanol content (vol%)	Temperature (℃)	Days	a	b
1	10	25	1 ~ 15	2.517	0.184
2	20	25	1 ~ 15	2.330	0.180
3	30	25	1 ~ 15	1.966	0.167
4	40	25	1 ~ 15	1.408	0.105
5	10	-20	1 ~ 15	1.008	0.519
6	20	-20	1 ~ 15	0.923	0.476
7	30	-20	1 ~ 15	0.535	0.491
8	40	-20	1 ~ 15	0.067	0.401
9	10	-20	15 ~ 220	1.911	0.164
10	20	-20	15~ 220	1.821	0.161
11	30	-20	15 ~ 220	1.303	0.184
12	40	-20	15 ~ 220	0.573	0.193

Table 2 | The calculated lifespans of LLG 1 under -20℃

Samples	Ethanol content (vol%)	Temperature (℃)	Lifespan (days)
1	10	-20	258
2	20	-20	310
3	30	-20	339
4	40	-20	593

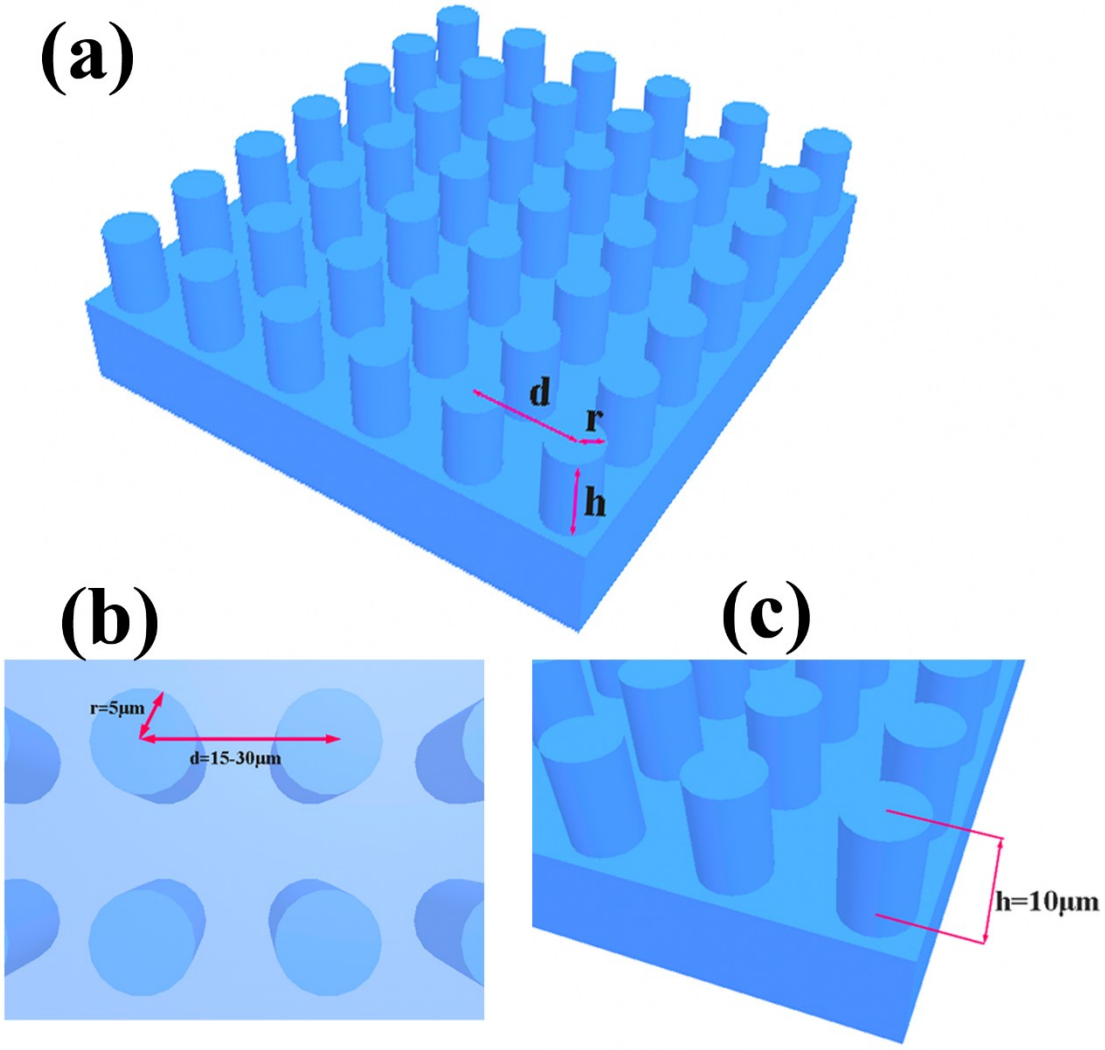

Supplementary Figure S8 | Schematic illustration of the detailed geometry of the pillars on the silicon wafer. r was the radius of pillar, **h** was the height of pillar, and **d** was the center distance between adjacent pillars. The value of **d** varied from 15 μm to 30μm. **(a)** the top view of the pillars. **(b)** the side view of the pillars.

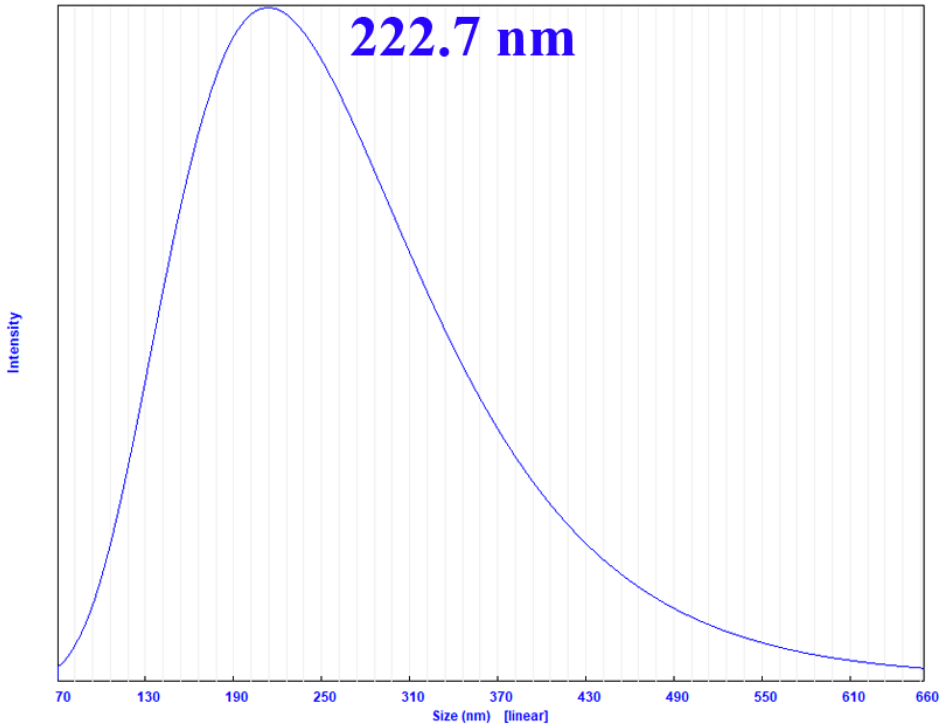

Supplementary Figure S9 | Diameter distribution of SiO_2 particles synthesized in this work. The particle size was in a unimodal distribution, with a mean size of 222.7nm.

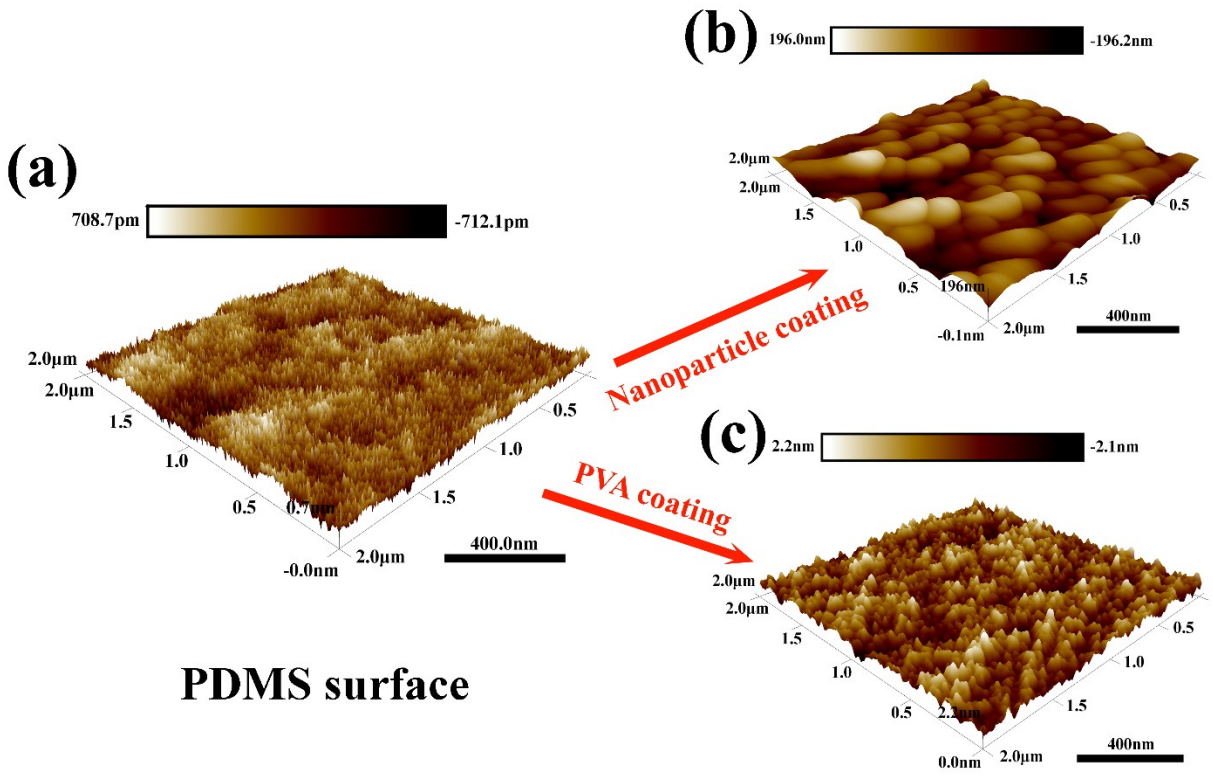

Supplementary Figure S10 | The AFM images showing the roughness of LLG 2 with and without surface treatment. (a) Roughness of PDMS surface as prepared. **(b)** Roughness of PDMS surface after treating with SiO_2 nanoparticles. **(c)** Roughness of PDMS surface after treating with PVA.

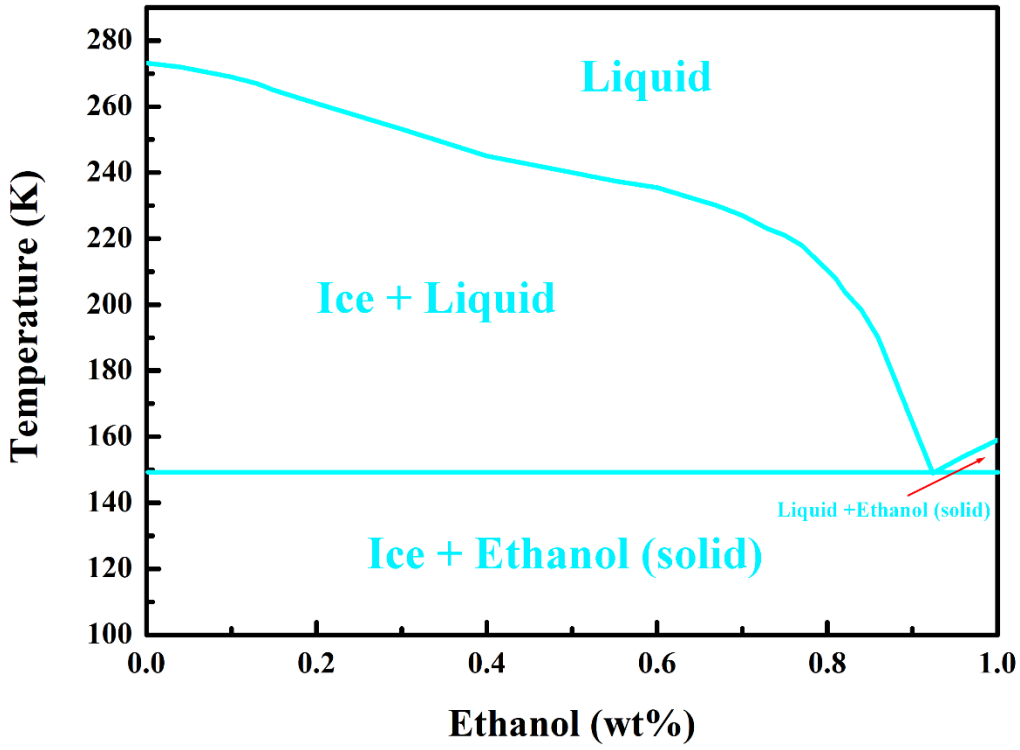

Supplementary Figure S11 | The phase diagram for the EtOH-H_2O system. The phase diagram of the EtOH-H_2O was a good supplement that help to explain why ethanol (or mixture of ethanol and water) could be a better lubricant layer compared to aqueous lubricant layer at low temperature[5-7]. The liquid phase contained both ethanol and water in the figure. Pure ethanol has less hydrogen bonds per unit volume than pure water. With addition of ethanol into water, the hydrogen bonds density in the liquid phase reduced, which finally resulted in lower ice adhesion strength in the one hand. In the second hand, the mixture solution of ethanol and water could effectively lower the freezing point of the liquid layer, maximally as low as 149K, which maintains lubricating effect to ice in a broad temperature range. Thus, LLG own high icephobic potential that can function well at extremely low temperature.

References

1. Z. He, S. Xiao, H. Gao, J. He and Z. Zhang, *Soft matter*, 2017, **13**, 6562-6568.
2. M. Nosonovsky and V. Hejazi, *ACS nano*, 2012, **6**, 8488-8491.
3. Z. He, Y. Zhuo, J. He and Z. Zhang, *Soft Matter*, 2018.
4. J. Chen, J. Liu, M. He, K. Li, D. Cui, Q. Zhang, X. Zeng, Y. Zhang, J. Wang and Y. Song, *Applied Physics Letters*, 2012, **101**, 111603.
5. R. Anderson, A. Chapoy, H. Haghighi and B. Tohidi, *The Journal of Physical Chemistry C*, 2009, **113**, 12602-12607.
6. A. Potts and D. Davidson, *The Journal of Physical Chemistry*, 1965, **69**, 996-1000.
7. P. Boutron and A. Kaufmann, *The Journal of Chemical Physics*, 1978, **68**, 5032-5041.